

ORIGINAL ARTICLE

3D angioarchitecture changes after spinal cord injury in rats using synchrotron radiation phase-contrast tomography

J Hu¹, Y Cao¹, T Wu¹, D Li¹ and H Lu²

Study design: A basic experiment study.

Objectives: An understanding of the three-dimensional (3D) angioarchitecture changes that occur after SCI will improve our knowledge of the pathogenesis of SCI and aid in the development of valuable therapeutic strategies to improve its poor outcomes. Our aim was to visualize the normal and traumatized spinal angioarchitecture in 3D using a high-resolution synchrotron radiation phase-contrast tomography (SR-PCT) and evaluate its diagnostic capability.

Setting: SCI Center of Xiangya Hospital of Central South University in China.

Methods: SR-PCT was used as novel high-resolution imaging tool to detect 3D morphological alterations in spinal cord microvasculature after injury.

Results: In a rat model, the morphology of the microvasculature on 2D digital slices was matched with histological findings in both the normal and injured spinal cord. 3D angioarchitecture changes after SCI were successfully obtained via SR-PCT without the use of a contrast agent. Quantitative analysis on 3D images of the injured spinal cord revealed a significant decrease in the number and volume of vascular networks. This was especially relevant to vessels with a diameter < 50 μm .

Conclusion: The 3D local blood supply to the spinal cord was severely disrupted after the acute violent injury. Our results indicate that the use of SR-PCT may improve our understanding of the pathogenesis of SCI and provide a new approach to the morphological investigation of neurovascular diseases in preclinical research.

Spinal Cord (2015) 53, 585–590; doi:10.1038/sc.2015.49; published online 31 March 2015

INTRODUCTION

The spinal cord microvasculature is a complex and delicate three-dimensional (3D) structure in the central nervous system. Under normal physiological conditions, the spinal cord microvasculature enables neural tissue to survive by providing necessary nutrition and maintaining a balanced local microenvironment.¹ Under the pathological process of a spinal cord injury (SCI), acute trauma can severely injure the spinal cord vasculature and result in irreversible damage to neurological function.² Revascularization following SCI is a complex process that involves remodeling of the number, connectivity, spatial distribution and direction of blood vessels, all of which affect the functional recovery of the spinal cord from trauma-induced ischemia.³

Knowledge of the 3D pathologic changes in the spinal cord microvasculature after SCI may aid in the development of valuable therapeutic strategies to improve its poor outcomes. Currently, there is a lack of effective imaging techniques for quantitative evaluation of the microvasculature difference in normal and injured spinal cord models. A number of studies have used 2D and 3D imaging to investigate the vascular response to SCI, but available technology is not sophisticated enough to provide clinically meaningful results.⁴ Micro-computed tomography is a powerful 3D imaging tool that is widely used to examine the morphology of various biomedical structures.⁵ However, low spatial resolution renders this tool unsuitable for accurate and complete 3D reconstruction of microvasculature.⁶ Furthermore, visualization of

microvasculature with micro-computed tomography requires the use of a contrast agent.⁷ As such, this technique has limited clinical use as patients may experience allergic reaction, renal impairment and even death in response to intravenous administration of a contrast agent.⁸

Phase contrast imaging (PCI) is increasingly used in biomedical applications.⁹ Unlike conventional attenuation-based X-ray imaging, PCI utilizes a unique refraction-based contrast mechanism that is suitable for the detection of soft biological tissue.¹⁰ Using a conventional X-ray tube source, PCI achieves better contrast in soft-tissue than conventional attenuation approaches.^{11–13} With the rapid development of X-ray sources of high tuneability, brightness and monochromaticity, the development of a new generation of X-ray imaging systems for medical applications has been stimulated. Synchrotron radiation-PCI, which uses SR as its probe, can generate enhanced contrast and good image quality, which allows vessel visualization. Compared with a laboratory X-ray source, SR-PCI can distinguish blood vessels with high spatial resolution at the micron level, without the need for a contrast agent.^{14,15} Combined with the CT algorithms, synchrotron radiation phase-contrast tomography (SR-PCT) can generate 3D representations, allowing to visualize the complexities of vascular microstructure, providing a new approach to the investigation and management of neurovascular disorders.

To date, SR-PCT has been widely used in experimental studies to reconstruct the microstructure of tissues and organs including nerve

¹Department of Spine Surgery, Xiangya Hospital, Central South University, Changsha, China and ²Department of Sports Medicine, Research Centre of Sports Medicine, Xiangya Hospital, Central South University, Changsha, China

Correspondence: Professor H Lu, Department of Sports Medicine, Xiangya Hospital, Central South University, Xiangya road No 87, Changsha 410008, PR China.

E-mail: hongbinlu@hotmail.com

Received 19 July 2014; revised 2 February 2015; accepted 6 February 2015; published online 31 March 2015

tissue, alveoli and kidney.^{16–18} Reports of the application of SR-PCT for neurovascular imaging are limited.¹⁹

In the present study, we used SR-PCT as a high-resolution imaging tool to investigate the 3D angioarchitecture of the normal spinal cord and the alterations associated with acute SCI. These data will inform the research and development of valuable diagnostic and therapeutic strategies to improve patient outcomes after SCI and other neurovascular disorders.

MATERIALS AND METHODS

Animals and sample preparation

Animals were obtained from the Experimental Center in Central South University. All care, treatment and surgical interventions of animals were conducted in compliance with the guidelines of the Animal Care and Use Committee of Central South University.

Male, Sprague–Dawley rats (250–300 g) were randomly divided into two groups ($n=8$ per group). Experimental group rats underwent laminotomy at the level of the 10th thoracic spinal vertebra, and a modified Allen's weight drop device was used to establish an incomplete SCI model.²⁰ A normal control group rats only underwent laminotomy. Twenty-four hours post injury, all animals were deeply anesthetized with an overdose of 10% chloral hydrate (3 ml kg^{-1}) intraperitoneally.

Imaging

Immunofluorescence. A thoracotomy was performed. Heparinized saline (500 ml) was rapidly perfused into the circulatory system via the aorta ascendens to allow effective draining of blood flow. Subsequently, four fresh spinal cord samples from each group at the level of the 10th thoracic spinal vertebra with a length of 4 cm were harvested. Sectioned ($10 \mu\text{m}$) and incubated overnight at 4°C with mouse anti-rat endothelial cell antigen-1 (RECA-1, 1:200; ABD Serotec, Oxford, UK), a specific microvessel endothelial cell marker. Tissue sections were labeled with fluorescent secondary antibodies

and examined with an Olympus BX60 microscope. Results were photographed and analyzed with PictureFrame software (Optronics), and these were compared with the vascular images obtained using SR-PCT.

Conventional X-ray imaging. An additional four spinal cord samples from each group were harvested and fixed with 4% paraformaldehyde, dehydrated using graded ethanol for 12–24 h, and scanned using conventional X-ray imaging (MX-20, Faxitron X-ray Corp., Wheeling, IL, USA). The scanning parameters were set to a peak voltage of 25 kVp and a current of 200 μA . The imaging pixel size was $50 \mu\text{m}$, and exposure time was set to 4 s. After obtaining a digital image of the spinal cord, the DICOM image software (Ver. 3., USA) was used to adjust image quality to facilitate improved observation over a reasonable range.

SR-PCT imaging. After conventional X-ray scanning, four animals from each group (experimental group and control normal group) were used for this experiment. Spinal cords were harvested from the same levels and cut into 1-cm lengths, designated regions of interest, and analyzed by SR-PCT at the Shanghai Synchrotron Radiation Facility. Images were captured at the Shanghai Synchrotron Radiation Facility BL13W1 Beamline (Figure 1). X-rays were generated from an electron storage ring with an accelerated energy of 3.5 GeV and an average beam current of 200 mA. The beamline covered a tunable energy spectrum ranging from 8 to 72.5 keV. In this CT test, the scanning energy was 15 keV. After penetrating the sample, the projections were magnified using diffraction-limited microscope optics ($\times 2$ magnification) with a $3.7 \times 3.7 \text{ mm}^2$ imaging field of view and digitized using a high-resolution 2048×2048 pixel CCD camera (pco.2000, PCO AG, Kelheim, Germany). The voxel size was $3.7 \times 3.7 \times 3.7 \mu\text{m}^3$, the exposure time was 2.0 s and the sample-to-detector distance was 30 cm. A total of 720 projection images were obtained by continuously rotating the samples from 0° to 180° . The total duration for the image acquisition process of one CT scan was ~ 35 min. Three CT scans were taken for 1-cm length of spinal cord in each sample. Original projection images were transformed into digital slices using the fast-slice CT reconstruction software (compiled by the BL13W1 experimental station) based on a filtered back projection algorithm. The 3D rendered images were reconstructed by sequential series of 2D slices with the VG Studio Max 3D reconstruction software (version 2.1, Volume Graphics GmbH, Heidelberg, Germany).

Histomorphological imaging. After SR-PCT image acquisition, tissue samples were dissected longitudinally in the vertical plane for histological assessment by hematoxylin-eosin staining. The spinal cord images were obtained using an optical microscope (Olympus BX51; Olympus, Tokyo, Japan), and these were compared with the images obtained using SR-PCT.

SR μ CT imaging and data analysis

Vessel segmentation. After scanning, the 3D image of each regions of interest was imported into Image J software (Rasband, W.S., National Institutes of Health, Bethesda, MA, USA) for blood vessel extraction and calculation of vascular morphological parameters. The vasculature was segmented from the

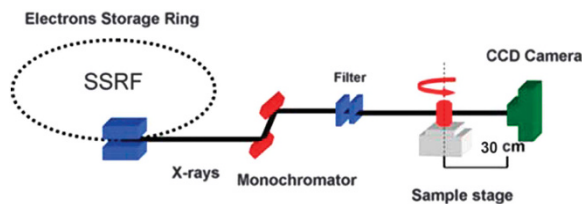


Figure 1 Schematic diagram of the BL13W1 beamline at Shanghai Synchrotron Radiation Facility (SSRF). A collimated 15 keV X-ray beam was monochromatized by a double Si (111) crystal system. Spinal cord samples were mounted on the rotary stage and positioned in the X-ray beam. An X-ray CCD camera captured 1024×1024 pixel (pixel size, $\sim 3.7 \times 3.7 \mu\text{m}^2$) phase-contrast X-ray images.

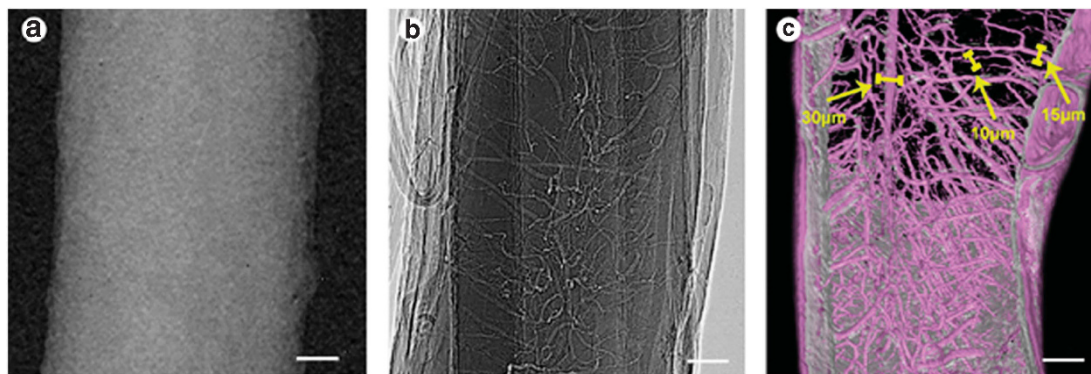


Figure 2 Images of spinal cord microvasculature. (a) Conventional X-ray images. (b) 2D SR-PCT projection images. (c) 3D SR-PCT render images. The smallest vessel that could be detected was $\sim 10 \mu\text{m}$ in diameter. Bars = $100 \mu\text{m}$.

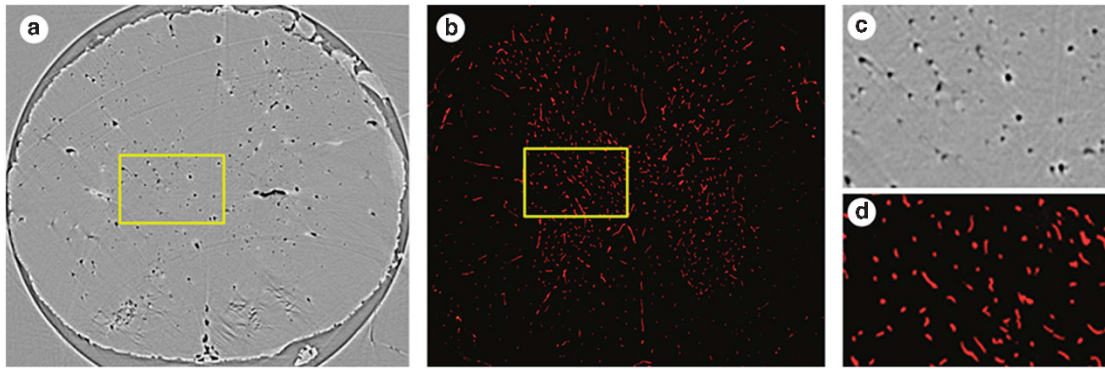


Figure 3 (a) SR-PCT slice images. (b) Immunofluorescence staining of microvessels. The red signal represents vessels with positive RECA-1 staining. (c, d) Magnified images of the yellow rectangles in (a) and (b).

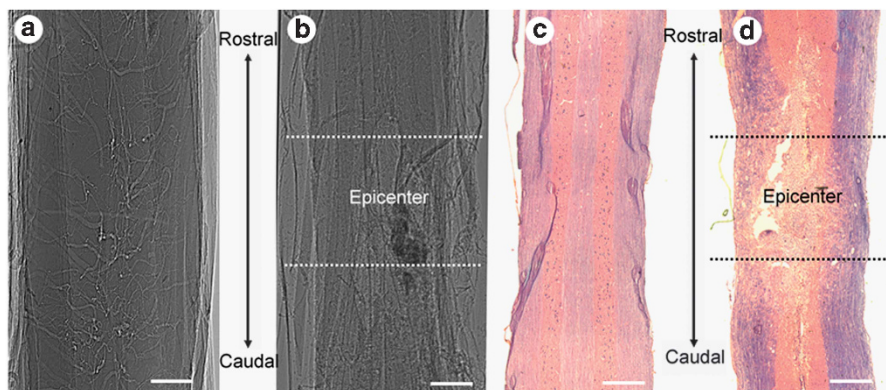


Figure 4 Pathological changes in microvasculature after SCI. (a, b) 2D SR-PCT projection images. (c, d) H&E staining. In normal spinal cord, the intramedullary region had a dense microvascular network (a) and the structure of the neural parenchyma was intact (c). In the damaged spinal cord, the trauma caused loss of neural tissue (d) accompanied by severe structural damage to the spinal cord microvasculature (b). The damaged area was not limited to the injured epicenter; it extended rostrally and caudally, forming a spindle shape on both sides at the periphery of the injury (b, d). Bars = 100 μ m.

tissue using an iterative gray level-based threshold algorithm.²¹ A binary 3D vascular structure was obtained. To eliminate small, disconnected objects and gaps in the vasculature, the binary image was subjected to a 3D size filter to remove isolated background and foreground regions smaller than three voxels.

Characterization of vascular morphology. After segmentation, several morphometric parameters of the vasculature were computed to characterize the 3D vascular architecture. The vascular volume of the regions of interest was determined by computing the fractional occupancy of the binary vascular structure within each regions of interest. The Image J '3D Skeletonization' plugin was used to automatically extract the vascular centerlines or 3D skeleton²² and compute vessel branch lengths and brunch number, which were considered the vessel number. To measure vessel radius, a 3D Euclidean distance map²³ of the vasculature was computed using the ChamferMap module in Amira (Mercury, Richmond, TX, USA). This Euclidean distance map represents the smallest distance between each vessel voxel and the background. Vessel radius was determined by multiplying the binary skeletonized image with the Euclidean distance map. Vessel diameter, vessel number and vascular volume were calculated and compared between experimental and normal control groups.

Data are reported as the mean \pm s.d. The paired *t*-test was used for comparisons between the two groups. Data were analyzed by SPSS 17.0. $P < 0.05$ was considered statistically significant.

RESULTS

Visualization of the normal spinal cord microvasculature

Conventional X-ray images could hardly detect the microvasculature of the normal spinal cord because of the limited imaging resolution of

this technique (Figure 2a). Two-dimensional SR-PCT projection images clearly visualized the microvascular network (Figure 2b). Vessel outlines were smooth, complete and continuous. The vessels appeared to overlap and form a dense network. 3D SR-PCT reconstruction images revealed the complexity of the spinal cord microvasculature (Figure 2c). This superior imaging technique detected vessels with diameters of 10 μ m, which could not be visualized using conventional imaging.

Immunofluorescence staining of RECA-1 in microvessel endothelial cells confirmed the accuracy of the SR-PCT reconstruction image. In the transverse section view of the spinal cord, positive RECA-1 staining (Figure 3b and d) corresponded with equivalent SR-PCT reconstruction slice data (Figure 3a and c).

2D SR-PCT images: pathological changes in microvasculature after SCI

2D SR-PCT projection images of the spinal cord microvasculature from rats in the control group are shown in Figure 4a. The microstructure of the intramedullary blood vessels was clearly visualized. Following SCI, the angioarchitecture of the spinal cord at the region of maximal injury (epicenter) had collapsed and disappeared. Damage to the microvasculature extended rostrally and caudally from the epicenter, forming a spindle shape on both sides at the periphery of the injury (Figure 4b). Hematoxylin-eosin stained normal and injured spinal cord tissue showed the shape of the injured

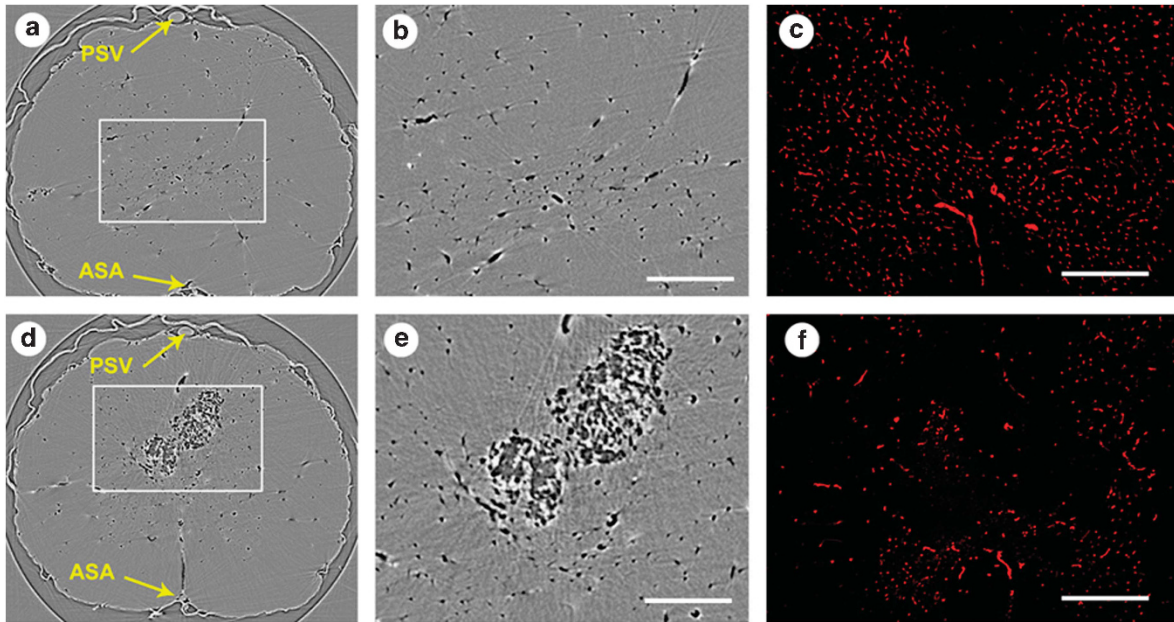


Figure 5 (a) 2D digital slice of the normal spinal cord. (b) Partial enlargement of (a) outlines a typical butterfly shaped region of gray matter with dense microvasculature. (d) 2D digital slice of a damaged spinal cord. (e) Partial enlargement of (d) reveals the damaged area and shows an absence of vascular structures. (c) Immunofluorescence staining of the normal spinal cord. (f) Immunofluorescence staining of the injured spinal cord. Similar morphological and pathological changes were seen with immunofluorescence. PSV, posterior spinal vein; ASA, anterior spinal artery. Bars = 100 μm .

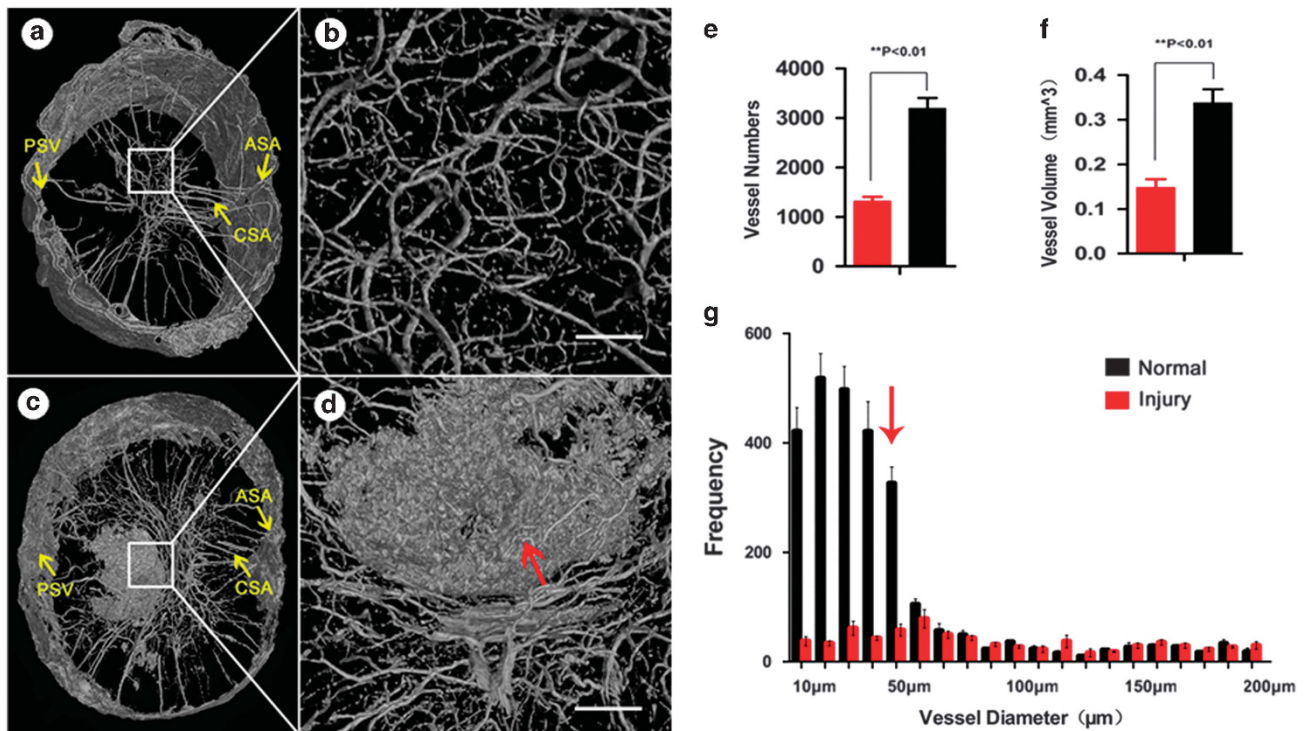


Figure 6 3D SR-PCT reconstruction images of angioarchitecture in normal spinal cord and after SCI. (a) 3D SR-PCT reconstruction image of normal spinal cord microvasculature. (b) Partial detail from (a). (c) 3D SR-PCT reconstruction image of the damaged spinal cord. (d) Partial detail from (c). The trauma formed a spindle shape on both sides at the periphery of the injury (c and d). The number (e) and volume of blood vessels (f) in the SCI rats were fewer and less than in control rats ($P < 0.01$). (g) The number of capillaries with diameter $< 50 \mu\text{m}$ (red arrow) was significantly decreased in SCI rats. PSV, posterior spinal vein; ASA, anterior spinal artery; CSA, central sulcus artery. Bars = 100 μm .

zone corresponded with the equivalent 2D SR-PCT projection image (Figure 4c and d); the intact structure of the neural parenchyma was lost following trauma (Figure 4d).

SR-PCT slices of the normal spinal cord demonstrated the butterfly outline of the spinal cord gray matter and showed intramedullary vasculature located in the gray matter; the microvascular density was reduced in the white matter (Figure 5a and b). SCI led to destruction and disappearance of the microvascular structure of the spinal cord. Both gray and white matters were injured, but the central gray matter suffered the most serious damage (Figure 5d and e). Similar pathological changes were observed with immunofluorescence (Figure 5c and f). The number of microvessels in the gray matter with positive RECA-1 staining was significantly decreased 24 h post SCI compared with the normal spinal cord. This reflected the degeneration or death of numerous endothelial cells due to the acute trauma (Figure 5c and f). These immunofluorescence results also confirmed the accuracy of the observations seen on the SR-PCT slices.

3D SR-PCT reconstruction images: angioarchitecture and quantitative analysis after SCI

3D SR-PCT reconstruction images of normal spinal cord microvasculature accurately represented the 3D morphology of the spinal cord microvasculature at the level of the 10th thoracic vertebra as reported in a previous study.²⁴ (Figure 6a and b) Two spinal arterial systems, the central sulcus arterial system and the peripheral arterial system, were clearly visualized in the 3D SR-PCT reconstruction images. The central sulcus arterial system was centrifugally distributed, and supplied the anterior horn of the spinal cord. The peripheral arterial system was concentrically arranged, and supplied part of the posterior horn of the spinal cord and most of the white matter (Figure 6a and b). Capillaries in the gray and white matter revealed a significant microvessel density gradient. The typical butterfly shape of the spinal cord gray matter was outlined within the capillary-dense areas. After SCI, the 3D microvasculature rapidly collapsed and disappeared. Although large extramedullary vessels (anterior spinal artery, posterior spinal vein) and vasculature in the white matter remained, many tiny blood vessels located in the gray matter were interrupted, dislocated and twisted. These observations suggest that the local blood supply to the spinal cord was severely disrupted after the acute violent injury, resulting in fatal damage to the neurons of the gray matter (Figure 6c and d).

3D SR-PCT reconstruction images allowed analysis and quantification of morphological parameters, including the number, volume and size of blood vessels, in normal and injured spinal cords. Injured spinal cord segments exhibited fewer vessels and a lower vessel volume compared with normal spinal cord segments ($P < 0.01$; Figure 6e and f). Importantly, the number of vessels with diameter $< 50 \mu\text{m}$ was significantly decreased in injured spinal cord segments (Figure 6g).

DISCUSSION

In this study, we successfully used 3D SR-PCT reconstruction images to demonstrate morphological changes in the angioarchitecture at the level of the 10th thoracic vertebra spinal cord in a SCI rat model. We showed that 3D SR-PCT reconstruction images can provide micrometer resolution of vessels in rat spinal cord without the use of a contrast agent. Furthermore, SR-PCT can present a large volume of digital information within a short period of time. Taken together, these data suggest that SR-PCT has preclinical significance as a research tool and clinical significance as a new noninvasive platform for imaging microvascular morphology during management of vascular pathologies.

Comparative analyses of 3D SR-PCT reconstruction images in normal and SCI rats revealed that acute trauma using a modified Allen's weight drop device directly damaged the intramedullary spinal cord vasculature. The vasculature at the injury epicenter suffered mechanical damage, including vascular rupture, occlusion, distortion and deformation. Trauma decreased the number and volume of spinal vessels, especially those with diameters $< 50 \mu\text{m}$.

Clinically, these data emphasize the importance of protecting the blood supply to the spinal cord following SCI. The changes to the microvasculature in our SCI rat model could be expected to markedly reduce blood flow through the spinal cord. Although the large extramedullary blood vessels were maintained, damage at the center of the gray matter was likely fatal for the neurons, which have a high metabolic demand and poor hypoxic resistance. Destruction of the intramedullary vessel network appeared to result in vascular endothelial cell dysfunction, which may further increase the extent of the ischemia and hypoxia. Indeed, the damaged region in our SCI rat model extended from the injury epicenter to the peripheral area, which is consistent with previous findings.⁴

Remodeling of spinal cord vasculature has an important role in the process of repair after SCI.²⁵ Posttraumatic spinal cord angiogenesis is a local metabolic adaptation to improve spinal cord ischemia. Studies have demonstrated temporary angiogenesis in the damaged and surrounding areas of the central nervous system at 3–7 days after trauma, a peak in angiogenesis at 7 days, and a gradual reduction thereafter. This incomplete short-term revascularization after trauma may alleviate the lack of blood perfusion.^{26,27} Despite these data, knowledge of the 3D morphological alterations in the microvasculature after acute SCI is limited. Further studies applying SR-PCT to evaluate the detailed time course of post-traumatic angiogenesis in 3D in our SCI rat model will be meaningful.

SR-PCT is associated with a number of limitations. In particular, the heartbeat makes it challenging to perform *in vivo* 3D imaging of microvessels. Despite this, the continued development of SR-PCT as a medical imaging technique may be a valuable method for the non-invasive detection of pathological microvascular morphology.

In conclusion, SR-PCT is a high-resolution imaging tool that can be used to monitor 3D morphological changes in the microvasculature following SCI. SR-PCT provides a new approach to the morphological investigation of neurovascular diseases in preclinical research, and may aid in the diagnosis and management of neurovascular disorders in clinical practice.

DATA ARCHIVING

There were no data to deposit.

CONFLICT OF INTEREST

The authors declare no conflict of interest.

ACKNOWLEDGEMENTS

This work was performed at the Shanghai Synchrotron Radiation Facility BL13W1, Shanghai, China, and was supported by the National Natural Science Foundation of China (No. 81171698, No. 81301542 and No. 81371956). We would like to thank Professor Tiqiao Xiao, Huiqiang Liu, for their kind assistance in SR-PCT measurements at the BL13W1 station.

1 Ashabi G, Ramin M, Azizi P. ERK and p38 inhibitors attenuate memory deficits and increase CREB phosphorylation and PGC-1 α levels in A β -injected rats. *Behav Brain Res* 2012; **232**: 165–173.

2 Mautes AE, Weinzierl MR, Donovan F, Noble LJ. Vascular events after spinal cord injury: contribution to secondary pathogenesis. *Phys Ther* 2000; **80**: 673–687.

- 3 Pries AR, Reglin B, Secomb TW. Structural adaptation of microvascular networks: functional roles of adaptive responses. *Am J Physiol Heart Circ Physiol* 2001; **281**: H1015–H1025.
- 4 Koyanagi I, Tator CH, Lea PJ. Three-dimensional analysis of the vascular system in the rat spinal cord with scanning electron microscopy of vascular corrosion casts. Part 2: acute spinal cord injury. *Neurosurgery* 1993; **33**: 285–292.
- 5 Schambach SJ, Bag S, Schilling L, Groden C, Brockmann MA. Application of micro-CT in small animal imaging. *Methods* 2010; **50**: 2–13.
- 6 Hu JZ, Wu TD, Zhang T, Zhao YF, Pang J, Lu HB. Three-dimensional alteration of microvasculature in a rat model of traumatic spinal cord injury. *J Neurosci Methods* 2012; **204**: 150–158.
- 7 Grabherr S, Hess A, Karolczak M, Thali MJ, Friess SD, Kalender WA. Angiophil-mediated visualization of the vascular system by microcomputed tomography: a feasibility study. *Microsc Res Tech* 2008; **71**: 551–556.
- 8 Caro JJ, Trindade E, McGregor M. The risks of death and of severe nonfatal reactions with high-vs low-osmolality contrast media: a meta-analysis. *Am J Roentgenol* 1991; **156**: 825–832.
- 9 Wilkins SW, Gureyev TE, Gao D, Pogany A, Stevenson AW. Phase-contrast imaging using polychromatic hard x-rays. *Nature* 1996; **384**: 335–338.
- 10 Arfelli F, Assante M, Bonvicini V, Bravin A, Cantatore G, Castelli E *et al*. Low-dose phase contrast x-ray medical imaging. *Phys Med Biol* 1998; **43**: 2845–2852.
- 11 Bech M, Jensen TH, Feidenhansl R, Bunk O, David C, Pfeiffer F. Soft-tissue phase-contrast tomography with an x-ray tube source. *Phys Med Biol* 2009; **54**: 2747–2753.
- 12 Hagen CK, Munro PR, Endrizzi M, Diemoz PC, Olivo A. Low-dose phase contrast tomography with conventional x-ray sources. *Med Phys* 2014; **41**: 070701.
- 13 Saam T, Herzen J, Hetterich H, Fill S, Willner M, Stockmar M. Translation of atherosclerotic plaque phase-contrast CT imaging from synchrotron radiation to a conventional lab-based X-ray source. *Plos One* 2013; **8**: e73513.
- 14 Bravin A, Coan P, Suortti P. X-ray phase-contrast imaging: from pre-clinical applications towards clinics. *Phys Med Biol* 2013; **58**: R1–35.
- 15 Zhang X, Liu XS, Yang XR, Chen SL, Zhu PP, Yuan QX. Mouse blood vessel imaging by in-line x-ray phase-contrast imaging. *Phys Med Biol* 2008; **53**: 5735–5743.
- 16 Beckmann F, Heise K, Kölsch B, Bonse U, Rajewsky MF, Bartscher M *et al*. Three-dimensional imaging of nerve tissue by x-ray phase-contrast microtomography. *Biophys J* 1999; **76**: 98–102.
- 17 Hwang J, Kim M, Kim S, Lee J. Quantifying morphological parameters of the terminal branching units in a mouse lung by phase contrast synchrotron radiation computed tomography. *PloS One* 2013; **8**: e63552.
- 18 Wu J, Takeda T, Lwin TT, Momose A, Sunaguchi N, Fukami T *et al*. Imaging renal structures by X-ray phase-contrast microtomography. *Kidney Int* 2009; **75**: 945–951.
- 19 Pinzer BR, Cacquevel M, Modregger P, McDonald SA, Bensadoun JC, Thuring T *et al*. Imaging brain amyloid deposition using grating-based differential phase contrast tomography. *Neuroimage* 2012; **61**: 1336–1346.
- 20 Allen AR. Surgery of experimental lesion of spinal cord equivalent to crush injury of fracture dislocation of spinal column: a preliminary report. *JAMA* 1911; **57**: 878–880.
- 21 Reichold J, Stampanoni M, Lena KA, Buck A, Jenny P, Weber B. Vascular graph model to simulate the cerebral blood flow in realistic vascular networks. *J Cereb Blood Flow Metab* 2009; **29**: 1429–1443.
- 22 Lee TC, Kashyap RL, Chu CN. Building skeleton models via 3-D medial surface/axis thinning algorithms. *Graph Model Im Proc* 1994; **56**: 462–478.
- 23 Tsai PS, Kaufhold JP, Blinder P, Friedman B, Drew PJ, Karten HJ *et al*. Correlations of neuronal and microvascular densities in murine cortex revealed by direct counting and colocalization of nuclei and vessels. *J Neurosci* 2009; **29**: 14553–14570.
- 24 Koyanagi I, Tator CH, Lea PJ. Three-dimensional analysis of the vascular system in the rat spinal cord with scanning electron microscopy of vascular corrosion casts. Part 1: Normal spinal cord. *Neurosurgery* 1993; **33**: 277–284.
- 25 Benton RL, Hagg T. Vascular pathology as potential therapeutic target in SCI. *Transl Stroke Res* 2011; **2**: 556–574.
- 26 Casella GT, Marcillo A, Bunge MB, Wood PM. New vascular tissue rapidly replaces neural parenchyma and vessels destroyed by a contusion injury to the rat spinal cord. *Exp Neurol* 2002; **173**: 63–76.
- 27 Loy DN, Crawford CH, Darnall JB, Burke DA, Onifer SM, Whittemore SR. Temporal progression of angiogenesis and basal lamina deposition after contusive spinal cord injury in the adult rat. *J Comp Neurol* 2002; **445**: 308–324.